Scientific Reports

https://doi.org/10.1038/s41598-026-39935-0

Article in Press

Investigation and enhancement of stress-dependent compliance characteristics in deep in-situ stress measurements based on anelastic strain recovery (ASR) method

Received: 31 August 2025

Accepted: 9 February 2026

Published online: 03 March 2026

Cite this article as: Li T., Xiang P., Ji H. *et al.* Investigation and enhancement of stress-dependent compliance characteristics in deep in-situ stress measurements based on anelastic strain recovery (ASR) method. *Sci Rep* (2026). https://doi.org/10.1038/s41598-026-39935-0

Tianyu Li, Peng Xiang, Hongguang Ji, Chang Li & Wei Wang

We are providing an unedited version of this manuscript to give early access to its findings. Before final publication, the manuscript will undergo further editing. Please note there may be errors present which affect the content, and all legal disclaimers apply.

If this paper is publishing under a Transparent Peer Review model then Peer Review reports will publish with the final article.

ARTICLE IN PRESS

© The Author(s) 2026. **Open Access** This article is licensed under a Creative Commons Attribution-NonCommercial-NoDerivatives 4.0 International License, which permits any non-commercial use, sharing, distribution and reproduction in any medium or format, as long as you give appropriate credit to the original author(s) and the source, provide a link to the Creative Commons licence, and indicate if you modified the licensed material. You do not have permission under this licence to share adapted material derived from this article or parts of it. The images or other third party material in this article are included in the article's Creative Commons licence, unless indicated otherwise in a credit line to the material. If material is not included in the article's Creative Commons licence and your intended use is not permitted by statutory regulation or exceeds the permitted use, you will need to obtain permission directly from the copyright holder. To view a copy of this licence, visit http://creativecommons.org/licenses/by-nc-nd/4.0/.

ARTICLE IN PRESS

Investigation and Enhancement of Stress-Dependent Compliance Characteristics in Deep In-Situ Stress Measurements Based on Anelastic Strain Recovery (ASR) Method

Tianyu Li [1,2], Peng Xiang [1,2,*], Hongguang Ji [1,2], Chang Li [3], Wei Wang [4]

1. Beijing Key Laboratory of Urban Underground Space Engineering, University of Science and Technology Beijing, Beijing 100083, China; ustblitianyu@163.com (T.L.); jihongguang@ces.ustb.edu.cn (H.J.)
2.National Engineering Research Center of Deep Shaft Construction, Beijing 100013, China
3 Shandong Gold Mining (Laizhou) Company Limited Sanshandao Gold Mine, Yantai 261400, China; 17806246157@163.com (C.L.)
4 China Coal Construction Group Third Engineering Department, Yantai 261400, China; 451921965@qq.com (W. W.)
* **Correspondence**: Peng Xiang, Beijing Key Laboratory of Urban Underground Space Engineering, University of Science and Technology Beijing, Beijing 100083, China. Email: xiangpeng811@126.com

ARTICLE IN PRESS

Abstract: To accurately obtain the deep in-situ stress state during the construction of deep vertical shafts, laboratory-based Anelastic Strain Recovery (ASR) compliance experiments were conducted. The results revealed that under uniaxial loading conditions, the shear and volumetric modes of ASR compliance tend to stabilize after 48 hours of unloading, and the extension of the loading time slows the rate of anelastic recovery. The ASR compliance and its ratio under different stress conditions (0.25 UCS and 0.5 UCS) varied with changes in stress. In-situ stress measurements based on the ASR method, conducted at the Sanshandao deep vertical shaft project site, showed that the ASR compliance under the 0.25 UCS stress condition provided stress values that more closely matched the results obtained from hydraulic fracturing, with the maximum principal stress deviation ranging from 0.14% to 4.1%, and the minimum principal stress deviation ranging from 0.27% to 4.57%. This study confirms that combining the depth of the sampled rock cores with in-situ stress conditions for compliance calibration can improve the accuracy of the ASR method. The findings provide foundational support for in-situ stress evaluation and rock mass stability control in similar deep strata.

ARTICLE IN PRESS

Keywords：In-situ stress measurement; ASR method; Anelastic strain recovery compliance; ASR measurement accuracy

1 Introduction

In-situ stress is the fundamental force responsible for deformation and failure in geotechnical excavation projects such as mining operations[1]. The escalating global demand for minerals and intensified excavation efforts have propelled the mining industry into progressively deeper environments[2-4]. Entry into these deep-seated strata is characterized by a shift in the in-situ stress field toward a quasi-hydrostatic state ($\sigma_h = \sigma_v$), a criterion proposed by Academician Xie Heping. This transition underscores the increasingly dominant role played by in-situ stress in governing the stability and behavior of deep rock masses[5]. Commonly used methods for in-situ stress testing include the hydraulic fracturing method, the stress relief method, and the Kaiser effect method, among which hydraulic fracturing and stress relief methods are more widely applied[6]. The Anelastic Strain Recovery (ASR) method was first proposed by Voight[7], and Teufel addressed the two-dimensional in-situ stress problem[8]. K. Matsuki introduced the use of six independent anelastic normal strains to determine three-dimensional in-situ stress, establishing a relationship between anelastic strain recovery compliance and the applied stress[9,10]. In 2007, Lin Weiren applied the ASR method to deep rock core testing, and the results were consistent with those obtained from other methods[11,12]. Following the Wenchuan earthquake, this method was applied for the first time in mainland China to measure in-situ stress in seismic fault zones via scientific drilling[13-17]. Li Zejie, Chen Tianxing, and others applied the ASR method to obtain the initial stress field in complex terrain for the Sichuan-Tibet Railway[18,19]. Zhang Xiaolin et al. compared the ASR method with hydraulic fracturing in a borehole over 2000 meters deep at Baoling Mountain, and the results showed good consistency[20]. Compared with other measurement methods, the ASR method offers advantages such as low cost, high efficiency, strong applicability, and no depth limitations, particularly in situations where methods like hydraulic fracturing cannot be used. Despite its significance, ASR compliance in geostress measurements is predominantly estimated via

ARTICLE IN PRESS

empirical assumptions—most notably the $J_{aS}(t)/J_{aV}(t)=2$ ratio[21]. The present study underscores the limitations of this simplification; applying this empirical constant to the Sanshandao ultra-deep shaft project resulted in discrepancies of 5.8% and 4.25% for the maximum and minimum principal stresses, respectively. While Sun[22] identified that ASR compliance is inherently rock-specific, conventional experimental benchmarks remain largely confined to 0.5 UCS stress levels. In deep-seated environments, however, rock masses under multi-field coupling manifest complex non-linear behaviors that diverge significantly from shallow formations[23]. Moreover, the intrinsic heterogeneity of rock under elevated stress regimes serves as a fundamental catalyst for the observed variability in macroscopic properties[24].However, current research on the stress-dependent compliance characteristics of deep rock using the ASR method remains limited, resulting in insufficient measurement accuracy and restricting the broader application of the ASR technique in in-situ stress determination. In this study, we investigate the ASR compliance of deep granite from a metal mine under different stress levels (0.25 UCS and 0.5 UCS) and loading durations (24 h and 48 h), aiming to analyze the relationship between ASR compliance, stress levels, and loading time. The mechanical mechanisms underlying the stress-dependent compliance characteristics of granite are further elucidated. Taking the Sanshandao Gold Mine's ultra-deep shaft project as a case study, we conduct a comparative analysis between in-situ stress measurements obtained by the hydraulic fracturing method and those derived from the ASR method. Based on these findings, we propose methodological improvements to enhance the accuracy of ASR-based stress measurements. The results of this research provide valuable insights and practical references for the convenient, cost-effective, and precise determination of deep in-situ stress states.

2 Anelastic Methods for In-situ Stress Measurement in Rock

2.1. Fundamental Principles of the Anelastic Strain Recovery (ASR) Method

Rock is a viscoelastic material that exhibits rheological behavior[25]. The Anelastic Strain Recovery (ASR) method is a deep in-situ stress measurement technique that leverages this

ARTICLE IN PRESS

rheological property by capturing the time-dependent recovery of anelastic strains in oriented rock cores[16]. As illustrated in Figure 1, when a core sample is extracted and the original triaxial stress state is released, the elastic deformation recovers instantaneously, while the anelastic strain recovery occurs gradually with a measurable time lag. By monitoring the temporal evolution of this anelastic strain recovery, it is possible to reconstruct the three-dimensional in-situ stress state of the rock mass.

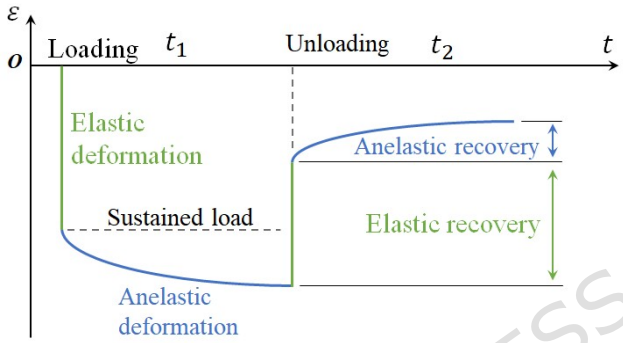

Figure 1. Time-Dependent Strain Behavior of Rock During Loading and Unloading Processes.

In the three-dimensional anelastic strain recovery theory proposed by the Japanese scholar Matsuki, when the stress tensor $(\sigma_x, \sigma_y, \sigma_z, \tau_{xy}, \tau_{yz}, \tau_{zx})$ is expressed in the Cartesian coordinate system and the pore pressure (l, m, n) is gradually released, the anelastic recovery of the average normal strain in an arbitrary direction $\varepsilon_a(t)$ can be expressed by Equation (1):

$$\varepsilon_{\mathrm{m}}(t) = \frac{1}{3}\begin{bmatrix}(3l^2-1)\sigma_x + (3m^2-1)\sigma_y + (3n^2-1)\sigma_z + \\ 6lm\tau_{xy} + 6mn\tau_{yz} + 6nl\tau_{zx}\end{bmatrix} J_{aS}(t) + (\sigma - P_0) J_{aV}(t) + \alpha_T \Delta T \quad (1)$$

In this equation, *l*, *m*, and *n* are the direction cosines corresponding to the arbitrary direction, defined with respect to the Cartesian axes X, Y, and Z. α_T denotes the linear thermal expansion coefficient; ΔT represents the temperature variation; σ_m is the average normal stress; P_0 denotes the pore water pressure; and $J_{aS}(t)$, $J_{aV}(t)$ refers to the ASR compliance, which includes both shear and volumetric compliance components.

By measuring anelastic normal strains in more than six independent directions and solving

ARTICLE IN PRESS

the corresponding system of equations, the three-dimensional in-situ stress tensor can be determined. Since the principal axes of the in-situ stress tensor coincide with those of the anelastic strain tensor, determining the orientation of the principal strains directly yields the orientation of the principal stresses.

Therefore, the three-dimensional in-situ stress tensor $\sigma_i (i = 1,2,3)$ can be obtained using Equation (2):

$$\sigma_i = e_i(t) / J_{aS}(t) + \left\{ e_m(t) - \alpha_T \Delta T(t) \right\} / J_{aV}(t) + P_0 \quad (2)$$

In this equation, $e_i = \varepsilon_i - e_m (i = 1,2,3)$ is principal strain deviation; $\varepsilon_i (i = 1,2,3)$ is three principal strains; $e_m = (\varepsilon_1 + \varepsilon_2 + \varepsilon_3)/3$ is average principal strain.

ARTICLE IN PRESS

2.2. Anelastic strain recovery compliances

The anelastic strain recovery compliances of rock—namely the volumetric compliance $J_{aV}(t)$ and the shear compliance $J_{aS}(t)$—are critical parameters for calculating in-situ stress using the ASR method. When the rock is assumed to behave as an isotropic medium, the direction of the principal stress deviators coincides with that of the principal stresses and the anelastic principal strains[26]. Therefore, one of the core steps in ASR-based stress determination is the calibration of the volumetric and shear recovery compliances. Under conventional triaxial testing conditions, these parameters can be expressed as shown in Equation (3):

$$\begin{aligned} J_{aV}(t) &= \frac{\varepsilon_{1a} + 2\varepsilon_{3a}}{\sigma_1 + 2\sigma_3} \\ J_{aS}(t) &= \frac{\varepsilon_{1a} - \varepsilon_{3a}}{\sigma_1 - \sigma_3} \end{aligned} \quad (3)$$

Where σ_1 and σ_3 denote the maximum and minimum principal stresses, respectively; ε_{1a} represents the axial anelastic recovery strain; and ε_{3a} denotes the circumferential (or lateral) anelastic recovery strain.

To simplify the determination of anelastic strain recovery compliance in the ASR method,

ARTICLE IN PRESS

Matsuki and colleagues proposed that the ratio *K* between the volumetric compliance ($J_{aS}(t)$) and the shear compliance ($J_{aV}(t)$) of rock tends to approach a constant value. Therefore, in practical ASR-based in-situ stress calculations, it is sufficient to determine the shear and volumetric compliances of the rock to accurately estimate the stress state.

3 Research on ASR Compliance Experiments of Deep Rock Cores

Characterizing the in-situ stress field via the anelastic strain recovery (ASR) technique necessitates the accurate determination of two fundamental constants: the shear ($J_{aS}(t)$) and volumetric ($J_{aV}(t)$) ASR compliances. Given that stress relief is most pronounced along the axis of vertical boreholes, Matsuki demonstrated that the $J_{aS}(t)/J_{aV}(t)$ ratio exhibits a convergent behavior under different stress conditions, thereby streamlining the experimental calibration process[27]. Accordingly, uniaxial loading-unloading cycles performed on rock specimens can reliably replicate the primary stress relief path. By incorporating the constitutive parameters obtained from these uniaxial tests into the material model, a robust inversion of the in-situ stress state can be achieved.

3.1. Loading System for ASR Compliance Experiments of Deep Rock Cores

The shear and volumetric mode compliances of the rock specimens were calibrated using a custom-built anelastic constant-load system. This apparatus consists of a constant-load tester, a hemispherical indenter, and supporting blocks, as illustrated in Figure. 2. The system features a lever ratio of 1:100 and can accommodate a maximum load of 56 kg in weights. Additionally, it is equipped with a secondary lever balance weight to counteract the pre-compression stress induced by the loading rod assembly. The loading rod is aligned perpendicularly to the loading platform, which, in conjunction with the hemispherical spacer, effectively minimizes eccentricity errors during the application of axial loads.

ARTICLE IN PRESS

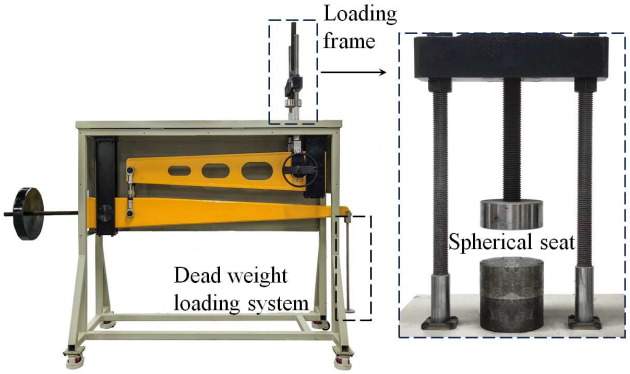

Figure 2. Anelastic constant-load system.

To ensure experimental continuity, the specimens designated for ASR compliance calibration were repurposed from rock cores following the completion of in-situ anelastic strain recovery measurements. While preserving the initial borehole core diameter of 30mm, these materials were precisely machined along their longitudinal axis into standard cylinders. These specimens adhere to a length-to-diameter ratio of 2, with specific dimensions of 30mm in diameter and 60mm in height, as depicted in Figure. 3.

Before commencing the experiments, each rock specimen underwent physical characterization, including density determination and ultrasonic pulse velocity (UPV) testing, to ascertain its structural homogeneity and integrity. Fundamental mechanical properties, specifically the elastic modulus and Poisson's ratio, were derived from uniaxial compression tests. To characterize the uniaxial compressive strength (UCS), standard specimens were prepared from intact rock blocks harvested from the same depth range (-1710 m to -1832 m) and positioned immediately adjacent to the ASR sampling sites. The comprehensive physical and mechanical attributes of these specimens are tabulated in Table 1.

Table 1. Physical properties of the rocks tested.

Physical property	ASR-1	ASR-2	ASR-3
Density (g/cm^3)	2.67	2.68	2.65
Elastic modulus (Gpa)	57.46	56.61	54.57
Poisson's ratio	0.16	0.15	0.15
Ultrasonic P-wave velocity (Km/s)	3.75	3.6	3.46
Ultrasonic S-wave Velocity (Km/s)	2.39	2.31	2.22
Average UCS (MPa)		158.6	

ARTICLE IN PRESS

The calibration experiment was conducted by machining the deep core rock samples into standard rock specimens of $\Phi\ 30\times60\text{mm}$, as shown in Figure 3. The surface of the standard rock specimens was polished and cleaned with alcohol, after which strain gauges were attached using AB epoxy resin and left to stand for more than 24 hours to ensure secure bonding and thermal equilibrium of the adhesive. As shown in Figure 4, two sets of strain gauges, labeled A and B, were symmetrically arranged along the front and back of the central part of the $\Phi\ 30\times60\text{mm}$ granite specimen. Each set of strain gauges consisted of one axial strain gauge and one hoop strain gauge.

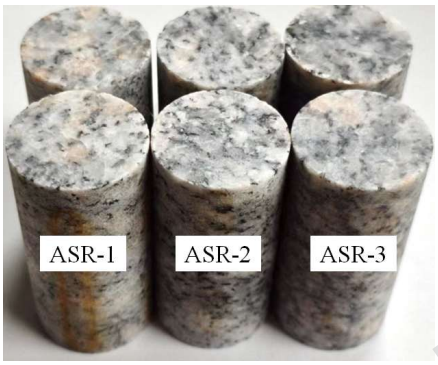

Figure 3. Anelastic Granite Specimen.

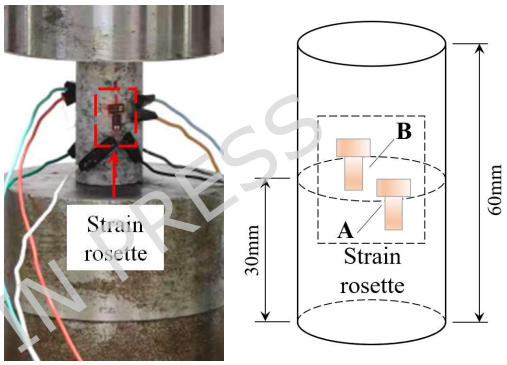

Figure 4. Photograph and Schematic Diagram of Specimen Layout.

The loading and anelastic recovery indoor experiments on the rock samples were conducted using an anelastic constant load system under uniaxial compression at atmospheric pressure. The experimental conditions were maintained at a constant indoor temperature. The entire experimental process included uniaxial compression, creep under constant load, unloading, and the anelastic recovery deformation after unloading, all of which were measured using strain gauges adhered to the surface of the specimens.

3.2. ASR Compliance Experiment Process and Recorded Curves of Deep Rock Cores

Before the commencement of loading, the horizontal alignment of the loading frame's crossbeam was meticulously calibrated with a spirit level to preclude any eccentric loading effects during axial force application. The loading protocol involved two distinct stress magnitudes: 0.25 UCS (39.8 MPa) and 0.5 UCS (79.6 MPa). The rationale for these specific

ARTICLE IN PRESS

thresholds is twofold: first, in-situ stress data from hydraulic fracturing within the -1000 m to -2000 m depth interval of the ultra-deep shaft indicates that the vertical principal stress σ_v -to-UCS ratio predominantly fluctuates between 0.15 and 0.35. Consequently, the 0.25 UCS level was chosen to accurately replicate the authentic in-situ vertical stress regime. Second, the 0.5 UCS level serves as a comparative benchmark, facilitating a direct correlation with standardized stress levels prevalent in existing literature.

The experimental protocol for each specimen set comprised four distinct loading cycles. Initial contact was established by slowly applying a seating load through the hemispherical indenter, succeeded by a progressive five-stage loading sequence. At a target stress of 0.25 UCS, each increment yielded an axial stress increase of 7.96 MPa, calibrated to the 1:100 leverage ratio and 5 kg mass units. For the 0.5 UCS regime, the incremental stress was adjusted to 15.92 MPa using 10 kg weights. The peak loads were held constant for intervals of 24 and 48 hours to allow for time-dependent deformation. Upon instantaneous unloading, the anelastic strain recovery was monitored for a subsequent 48-hour period. The temporal evolution of the axial stress throughout the test procedure is depicted in Figure. 5.

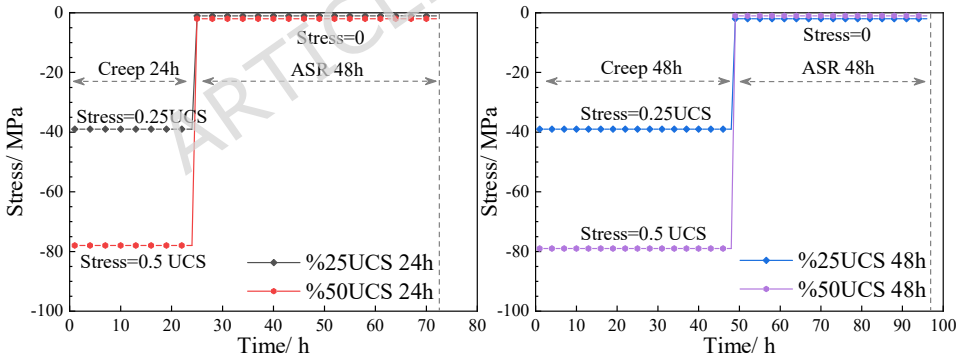

Figure 5. Axial Stress Curve with Time.

As shown in Figure 6, the total anelastic strain curves during loading and unloading for three groups of granite specimens are presented, which include both the instantaneous strain during loading and unloading and the anelastic strain. During the early stages of constant compressive load, the axial anelastic compressive strain increases significantly, while the corresponding hoop strain is tensile, and the rate of increase is relatively slow. After the rapid unloading of the axial load, the axial strain becomes tensile, and the hoop strain becomes

ARTICLE IN PRESS

compressive. The deformation after unloading recovery represents the anelastic recovery. Approximately 48 hours after complete unloading, the deformation reaches a stable state.

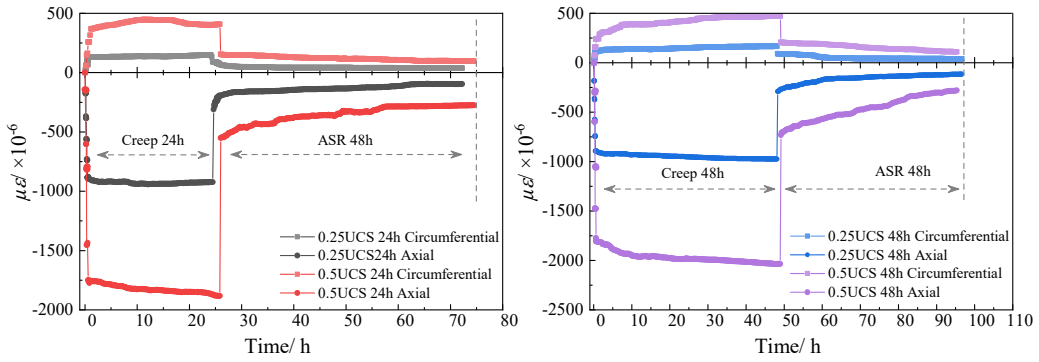

(a) ASR-1 Anelastic strain curve of specimen loading and unloading

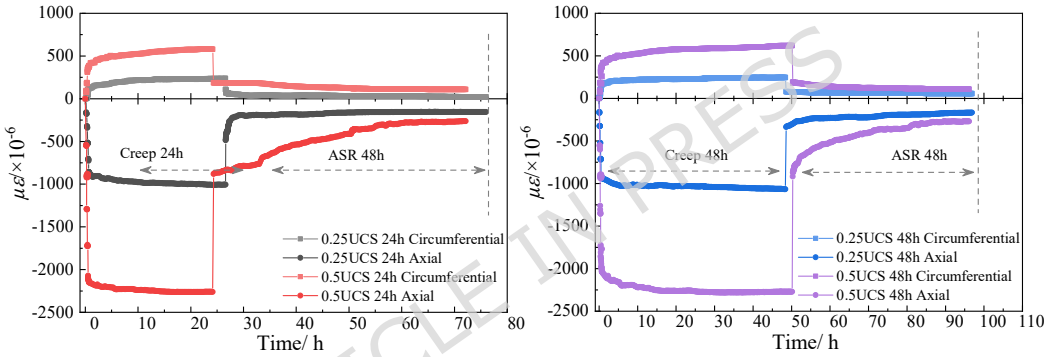

(b) ASR-2 Anelastic strain curve of specimen loading and unloading

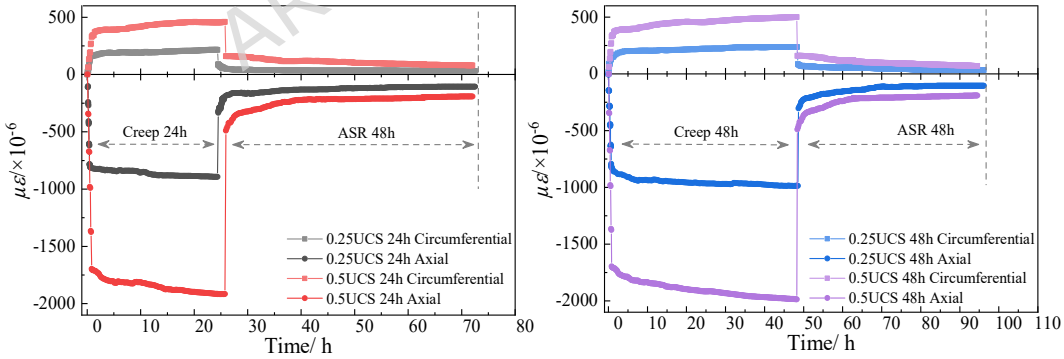

(c) ASR-3 Anelastic strain curve of specimen loading and unloading

Figure 6. Unloaded anelastic strain curves of three sets of specimens.

3.3. ASR Compliance Calibration of Deep Rock Cores

The ASR compliance results of the three groups of rock samples are presented in Figure 7. The findings indicate that the rate of change in ASR compliance decreases over time. Under

ARTICLE IN PRESS

the same applied stress level, samples subjected to long-term loading exhibit a lower rate of ASR compliance change compared to those under short-term loading, although both ultimately converge toward a stable value. The experimental results indicate that shear ASR compliance consistently outstrips its volumetric counterpart. Mechanistically, the anelastic strain recovery observed during unloading is predominantly governed by the reopening of previously compressed micro-cracks and frictional slippage across crack interfaces. These mechanisms facilitate localized morphological changes while exerting a minimal effect on the bulk volume of the rock. Moreover, elevated loading stresses exacerbate the formation of induced micro-fractures and grain-boundary sliding during the pre-unloading stage, thereby accumulating substantial shear-induced anelastic strain. This is macroscopically manifested as the sustained superiority of $J_{aS}(t)$ over $J_{aV}(t)$ and underscores the stress-dependent nature of the rock's anelastic properties.

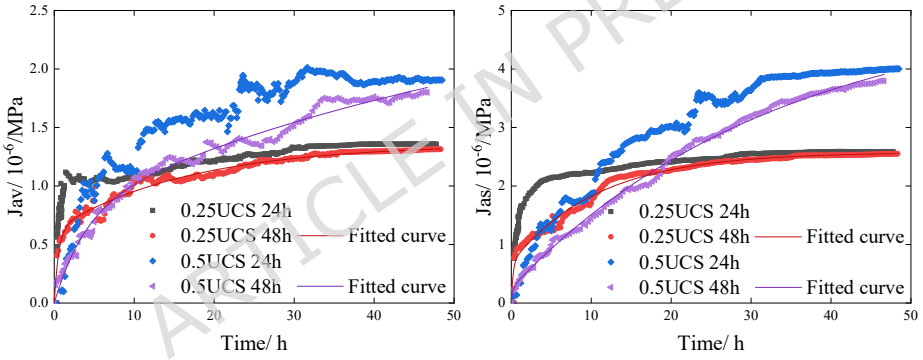

(a) ASR compliance and fitted curves of ASR-1 specimens under four stress loading conditions

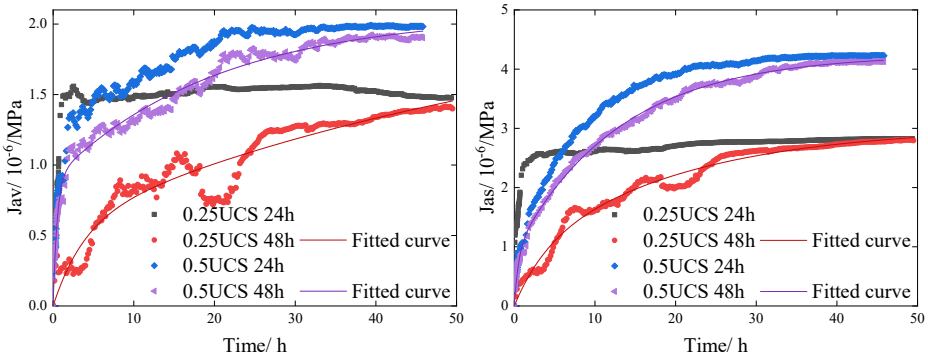

(b) ASR compliance and fitted curves of ASR-2 specimens under four stress loading conditions

ARTICLE IN PRESS

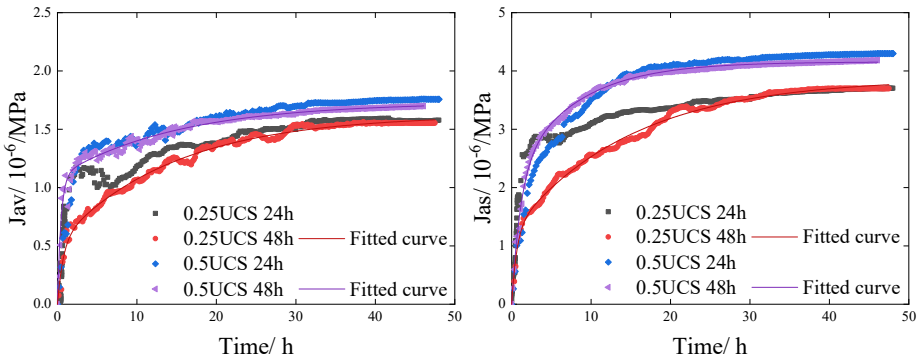

(c) ASR compliance and fitted curves of ASR-3 specimens under four stress loading conditions

Figure 7. ASR compliance of three sets of specimens under four stress loading conditions.

According to the experimental results shown in Figure 7, under different stress conditions, the shear and volumetric compliance of the three groups of rock samples gradually converge to a stable range within 48 hours after unloading, approaching a nearly constant value. The test data indicate that the ratio of anelastic strain recovery compliance between shear and volumetric modes for the three granite sample groups ranges from 1.85 to 2.48 (Table 2), which is generally consistent with previously reported values of $J_{aS}(t)/J_{aV}(t)=2$ although some deviations are observed. These discrepancies can be attributed to differences in the in-situ burial depth, mineral composition, and pore structure of the three sample groups, which lead to variations in the anelastic recovery deformation behavior after unloading. Nevertheless, all samples exhibit a broadly similar trend of anelastic recovery deformation.

Table 2. Comparison of Core Compliance Ratios Under Different Stress Conditions.

Granite specimen	Loading stress 0.25UCS		Loading stress 0.5UCS		Common estimates
	Maintain 24h	Maintain 48h	Maintain 24h	Maintain 48h	
ASR-1	1.85	1.87	1.94	1.95	2
ASR-2	1.91	1.98	2.13	2.16	2
ASR-3	2.34	2.38	2.45	2.48	2

3.4 Rheological Model of ASR Compliance for Deep Rock Cores

The ASR compliance in shear and volumetric modes for rock specimens can be fitted using the Kelvin rock rheological model. Since the anelastic recovery deformation of the rock can be divided into an initial stage and the entire process after the initial stage, a four-element Kelvin

ARTICLE IN PRESS

body model, consisting of two Kelvin bodies in series (Figure 8), is adopted. This model exhibits no instantaneous elasticity and no residual deformation, and it effectively reflects the anelastic deformation after unloading.

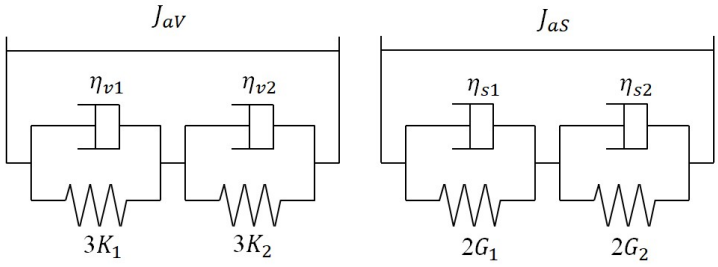

(a) Bulk Modulus four-element Units; (b) Shear Modulus four-element Units

Figure 8. Four-Element Kelvin Model for ASR Compliance.

Constitutive equation of the four-element Kelvin Model:

$$J_{aV}(t)=\frac{1}{3K_1}\left[1-\exp\left(-3K_1t/\eta_{v1}\right)\right]+\frac{1}{3K_2}\left[1-\exp\left(-3K_2t/\eta_{v2}\right)\right] \quad (4)$$

$$J_{aS}(t)=\frac{1}{2G_1}\left[1-\exp\left(-2G_1t/\eta_{s1}\right)\right]+\frac{1}{2G_2}\left[1-\exp\left(-2G_2t/\eta_{s2}\right)\right] \quad (5)$$

Where, $3K_i$ and $2G_i$ (for i=1,2) represent the elastic moduli of the Kelvin elements in volumetric and shear modes, respectively, while $\eta_{v1},\eta_{v2},\eta_{s1},\eta_{s2}$ denotes the corresponding viscous parameters.

The fitting results demonstrate that the experimental ASR compliance data are well described by the four-element Kelvin model. Based on the fitted parameters, the ASR compliances in shear and volumetric modes at the theoretical recovery limit ($T=\infty$) were calculated for all three groups of rock specimens under different stress conditions. The corresponding compliance ratios were also derived. The parameter fitting results are summarized in Table 3.

Table 3. Fitting Results of the Four-Element Kelvin Model for ASR Compliance.

Granite specimen	ASR-1		ASR-2		ASR-3	
	0.25UCS	0.5UCS	0.25UCS	0.5UCS	0.25UCS	0.5UCS
$J_{aV}(t)$	1.374	1.876	1.423	1.902	1.55	1.69

ARTICLE IN PRESS

(10^{-6}/MPa)						
$J_{aS}(t)$ (10^{-6}/MPa)	2.58	3.679	2.819	4.127	3.698	4.113
K_1 (MPa)	0.454	0.161	0.2	0.285	0.344	0.305
η_{v1} (MPa*h)	0.863	4.98	6.541	0.552	0.979	0.404
K_2(MPa)	0.534	0.635	0.578	0.369	0.455	0.522
η_{v2} (MPa*h)	22.88	30.78	39.761	17.317	31.242	23.66
R^2	0.972	0.986	0.912	0.988	0.958	0.979
G_1 (MPa)	0.264	0.103	0.22	0.149	0.185	0.227
η_{s1} (MPa*h)	0.321	0.797	4.529	0.568	0.337	0.509
G_2(MPa)	0.732	1.979	0.64	0.547	0.427	0.255
η_{s2} (MPa*h)	5.71	6.866	9.002	3.889	19.539	3.982
R^2	0.984	0.997	0.978	0.998	0.991	0.997
As T=∞						
$J_{aV}(t)$ (10^{-6}/MPa)	1.426	2.595	2.041	2.173	1.702	1.731
$J_{aS}(t)$ (10^{-6}/MPa)	2.706	5.107	4.054	4.715	4.052	4.295
$J_{aS}(t)/J_{aV}(t)$	1.897	1.968	1.986	2.169	2.381	2.481

The experimental results demonstrate that under the same uniaxial stress, although the three groups of samples were subjected to different loading durations (24 h and 48 h), both the shear and volumetric ASR compliance tended to stabilize within 48 hours after unloading. Prolonged loading duration was found to reduce the rate of anelastic recovery following unloading. However, under different stress conditions (0.25 UCS and 0.5 UCS), the shear and volumetric ASR compliance, as well as their ratios, varied for each sample group, exhibiting clear stress-dependent characteristics. Therefore, when employing the ASR method for in-situ stress measurements under deep geological conditions, it is essential to account for the influence of loading stress on the calibration of compliance.

ARTICLE IN PRESS

4 Research on the Improvement of ASR Method for Core Sampling-Based Borehole Stress Measurement

4.1 In-situ Stress Measurement Plan Using ASR Method for Deep Vertical Shafts

The project area is located in the ultra-deep vertical shaft of the Xishan mining district at the Sanshandao Gold Mine(Figure 9), with a depth exceeding 2000 meters. In response to the engineering conditions of the ultra-deep, high stress, complex strata, and uncompleted shaft, core sampling was performed at the -1710m working face during the construction of the deep vertical shaft. The ASR method was then used to measure in-situ stress in the depth range from -1710m to -1832m, based on the requirements for in-situ stress testing.

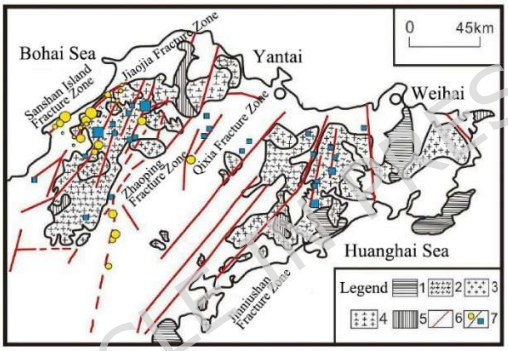

Figure 9. Regional Geological Structure of the Xishan Mining Area, Sanshandao Gold Mine.

Rock cores, surpassing 150 mm in length, were retrieved from the deep formations using a vertical drilling technique. Following a meticulous surface cleaning process, the specimens were equipped with a sensor array comprising four acoustic emission (AE) sensors and five strain gauge clusters, as per the spatial configuration depicted in Figure. 10.

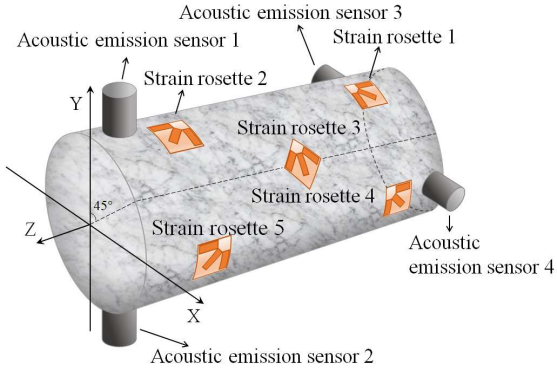

(a) Sensor Arrangement Schematic

ARTICLE IN PRESS

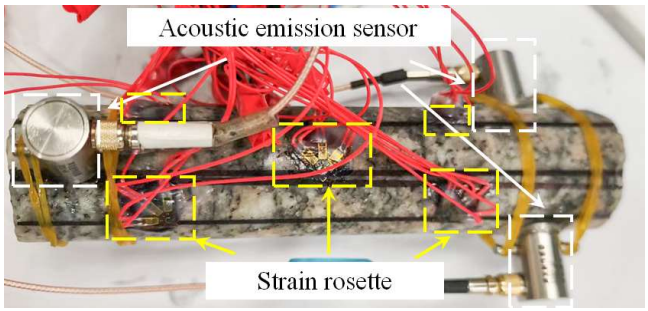

(b) Sensor arrangement

Figure 10. Sensor Layout Scheme for In Situ Unloading Rock Core.

Let the core coordinate system be defined as *O*—*XYZ*, as shown in Figure. 10(a). The *Z*—axis corresponds to the vertical direction in the field. Consequently, the relationship between the strain values measured by the strain gauges attached to the core surface and the strain tensor components $\varepsilon_x, \varepsilon_y, \varepsilon_z, \varepsilon_{xy}, \varepsilon_{yz}, \varepsilon_{zx}$ can be expressed as:

$$A\varepsilon = b \tag{6}$$

Where $\varepsilon = [\varepsilon_x, \varepsilon_y, \varepsilon_z, \varepsilon_{xy}, \varepsilon_{yz}, \varepsilon_{zx}]^T$ represents the strain tensor of the rock defined in the coordinate system shown in Figure. 10; $b = [b_1, b_2, b_3, b_4, b_5, b_6, b_7, b_8, b_9, b_{10}, b_{11}, b_{12}, b_{13}, b_{14}, b_{15}]^T$ denotes the strain values measured by the strain gauges attached to the core surface; and *A* is the coefficient matrix.

The expansion of the coefficient matrix *A* within this coordinate system is calculated as:

$$A = \begin{bmatrix} l_1^2 & m_1^2 & n_1^2 & 2l_1m_1 & 2m_1n_1 & 2n_1l_1 \\ l_2^2 & m_2^2 & n_2^2 & 2l_2m_2 & 2m_2n_2 & 2n_2l_2 \\ l_3^2 & m_3^2 & n_3^2 & 2l_3m_3 & 2m_3n_3 & 2n_3l_3 \\ l_4^2 & m_4^2 & n_4^2 & 2l_4m_4 & 2m_4n_4 & 2n_4l_4 \\ l_5^2 & m_5^2 & n_5^2 & 2l_5m_5 & 2m_5n_5 & 2n_5l_5 \\ l_6^2 & m_6^2 & n_6^2 & 2l_6m_6 & 2m_6n_6 & 2n_6l_6 \\ l_7^2 & m_7^2 & n_7^2 & 2l_7m_7 & 2m_7n_7 & 2n_7l_7 \\ l_8^2 & m_8^2 & n_8^2 & 2l_8m_8 & 2m_8n_8 & 2n_8l_8 \\ l_9^2 & m_9^2 & n_9^2 & 2l_9m_9 & 2m_9n_9 & 2n_9l_9 \\ l_{10}^2 & m_{10}^2 & n_{10}^2 & 2l_{10}m_{10} & 2m_{10}n_{10} & 2n_{10}l_{10} \\ l_{11}^2 & m_{11}^2 & n_{11}^2 & 2l_{11}m_{11} & 2m_{11}n_{11} & 2n_{11}l_{11} \\ l_{12}^2 & m_{12}^2 & n_{12}^2 & 2l_{12}m_{12} & 2m_{12}n_{12} & 2n_{12}l_{12} \\ l_{13}^2 & m_{13}^2 & n_{13}^2 & 2l_{13}m_{13} & 2m_{13}n_{13} & 2n_{13}l_{13} \\ l_{14}^2 & m_{14}^2 & n_{14}^2 & 2l_{14}m_{14} & 2m_{14}n_{14} & 2n_{14}l_{14} \\ l_{15}^2 & m_{15}^2 & n_{15}^2 & 2l_{15}m_{15} & 2m_{15}n_{15} & 2n_{15}l_{15} \end{bmatrix} = \begin{bmatrix} 0 & 0 & 1 & 0 & 0 & 0 \\ 0.5 & 0 & 0.5 & 0 & 0 & -1 \\ 1 & 0 & 0 & 0 & 0 & 0 \\ 1 & 0 & 0 & 0 & 0 & 0 \\ 0.5 & 0 & 0.5 & 0 & 0 & 1 \\ 0 & 0 & 1 & 0 & 0 & 0 \\ 0.25 & 0.25 & 0.5 & 0.5 & -0.707 & -0.707 \\ 0.5 & 0.5 & 0 & -1 & 0 & 0 \\ 0.25 & 0.25 & 0.5 & 0.5 & 0.707 & 0.707 \\ 0 & 0 & 1 & 0 & 0 & 0 \\ 0 & 0.5 & 0.5 & 0 & 1 & 0 \\ 0 & 1 & 0 & 0 & 0 & 0 \\ 0 & 1 & 0 & 0 & 0 & 0 \\ 0 & 0.5 & 0.5 & 0 & -1 & 0 \\ 0 & 0 & 1 & 0 & 0 & 0 \end{bmatrix} \tag{7}$$

ARTICLE IN PRESS

where l_i, m_i, n_i are the direction cosines of the *i*-th strain gauge axis relative to the axes of the *O—XYZ* coordinate system.

The number of unknowns in the strain component equations is $n = 6$, while the number of independent equations is $m = 9$. By applying the least squares method to solve this overdetermined system of equations, the following result can be obtained:

$$\varepsilon = \left(A^T A\right)^{-1} A^T b \tag{8}$$

The solution yields three eigenvalues, which represent the three principal strains ($\varepsilon_1, \varepsilon_2, \varepsilon_3$). By substituting these values back into the equations, the corresponding eigenvectors can be obtained, representing the direction cosines $l_i, m_i, n_i (i = 1, 2, 3)$ for each principal strain $\varepsilon_i (i = 1, 2, 3)$. The orientation of these principal strains, specifically the azimuth $D_i = \arctan(m_i / l_i)$ and inclination $V_i = \arcsin(n_i)$, can then be calculated from these direction cosines.

The monitoring layout scheme for the engineering site is shown in Figure 11, which includes a deformation monitoring system, an acoustic monitoring system, a constant temperature system, and an information collection and processing system. The Donghua DH3816N dynamic stress-strain testing and analysis system, combined with the DHDAS dynamic signal acquisition and analysis system, is used to collect and analyze the rock core strain recovery values. During the measurement process, core samples from the same borehole are used as temperature compensation samples to eliminate temperature effects. The constant temperature system utilizes the HH-420 high-precision water bath thermostat. The acoustic monitoring system uses the PCI-2 acoustic emission equipment to collect signals throughout the entire rock core strain recovery process. To avoid environmental noise interference, a threshold value of 45 dB is set. To ensure close contact between the rock sample and the acoustic emission sensor, petroleum jelly is used as a coupling agent, and the sensor is fixed with self-adhesive tape. Once the core sensors are arranged, they are connected to the strain acquisition instrument, and all channels are balanced. Acoustic emission monitoring is then initiated. After sealing the rock core for waterproofing, it is placed into the constant temperature water bath

ARTICLE IN PRESS

system. Data collection is stopped, and the core is removed once the strain data stabilizes or no more acoustic emission signals are detected.

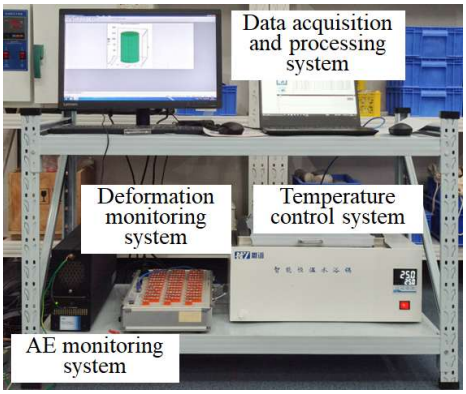

Figure 11. Integrated Monitoring System for In Situ Stress: Combined Acoustic Emission and ASR Method

4.2 Anelastic Strain Recovery Behavior of Core Sampling Rock Samples

Three intact core segments were selected from the borehole for ASR testing. Sample ASR-1 was obtained from a depth of 1722 m with a core length of 173 mm; ASR-2 was taken from 1744 m with a length of 172 mm; and ASR-3 was collected at 1831 m with a length of 196 mm. All specimens consisted of monzogranite and were continuously monitored for a duration of 72 hours.

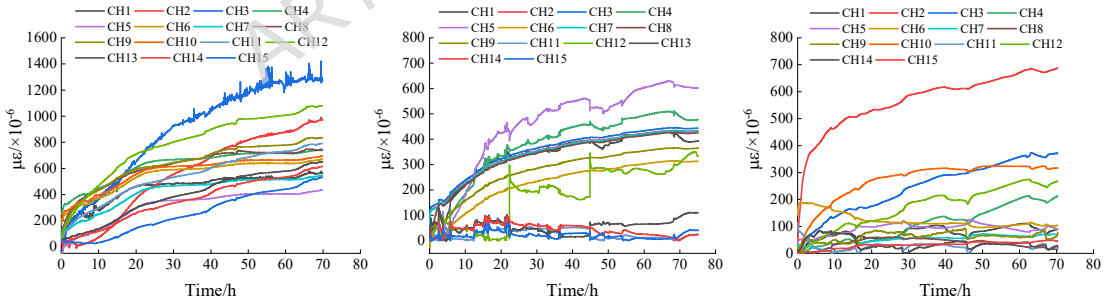

（a）ASR-1　　（b）ASR-2　　（c）ASR-3

Figure 12. Anelastic Strain Recovery Behavior of Rock Core Samples.

Figure 12 shows the anelastic strain-time curves for three core samples. The data from the CH3 channel of the ASR-1 specimen fluctuated significantly, but the trend was generally consistent with other channels. The CH10 channel data from the ASR-2 specimen exhibited large drift and was therefore discarded. Similarly, the CH13 channel data from the ASR-3

ARTICLE IN PRESS

specimen also showed considerable drift, leading to the exclusion of this data. After the rock cores were removed from their in-situ state, the anelastic strain initially changed rapidly but gradually flattened out over time. After 70 hours, the anelastic recovery strain reached its peak value and remained nearly constant. Significant differences in anelastic strain recovery were observed across different strain axes, which are related to the varying axial stress conditions experienced by the cores under in-situ stress. The direction with the largest component of the in-situ stress tensor exhibited a correspondingly larger anelastic strain recovery.

4.3 In-situ Stress Calculation Results Based on Different ASR Compliance Ratios

According to the Kelvin model illustrated in Figure. 1, the post-unloading strain exhibits an asymptotic behavior over time, reaching a plateau that indicates the cessation of anelastic recovery. Based on this characteristic, strain magnitudes recorded during the stabilized phase of each effective channel were extracted. By integrating these values with the calibrated ASR compliance, the in-situ stress states at various depths were quantified. To evaluate the accuracy of the proposed method, these findings were benchmarked against calculations derived from the conventional compliance ratio of 2 (refer to Table 4).

Table 4. In-situ stress calculation results corresponding to different compliance ratios.

Depth/m	$J_{aS}(t)/J_{aV}(t)$	σ_H/MPa	σ_h/MPa	σ_v/MPa
1722(ASR-1)	1.968（0.5UCS）	59.61	40.81	44.73
	1.897（0.25UCS）	59.63	40.80	44.72
	2（Commonly used estimates）	59.29	40.59	44.64
1744(ASR-2)	2.169（0.5UCS）	59.95	40.72	44.93
	1.986（0.25UCS）	60.92	41.13	45.13
	2（Commonly used estimates）	60.91	41.08	45.11
1831(ASR-3)	2.481（0.5UCS）	65.43	43.88	50.77
	2.381（0.25UCS）	65.93	44.06	51.08
	2（Commonly used estimates）	69.88	44.99	51.48

As shown in Table 3, the in-situ stress results derived using ASR compliance ratios calibrated under different stress conditions deviate from those obtained using the commonly assumed compliance ratio of 2. This discrepancy indicates that the compliance ratio has a

ARTICLE IN PRESS

significant influence on in-situ stress measurements using the ASR method.

4.4 Comparison Between the ASR Method and the Hydraulic Fracturing Technique

Hydraulic fracturing is one of the principal in-situ stress measurement methods recommended by the International Society for Rock Mechanics[28]. In the Xishan ore district of the Sanshandao gold mine, in-situ stress measurements were conducted using the SY-2007 stress testing system. A total of 23 hydraulic fracturing tests, including three impression packer tests, were performed across depths ranging from -300 m to -2000 m. The measurement system and field setup are illustrated in Figure 13.

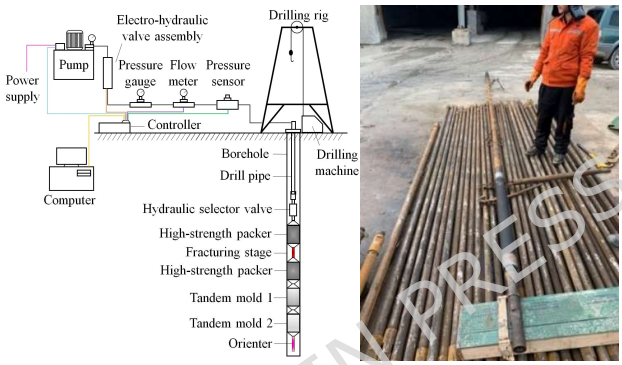

(a) SY-2007 hydraulic fracturing measurement system (b) Field measurements

Figure 13. Hydraulic Fracturing Field Tests.

The in-situ stress data obtained from hydraulic fracturing tests were used as a reference to compare with the stress measurements derived from the ASR method, as shown in Figure 14.

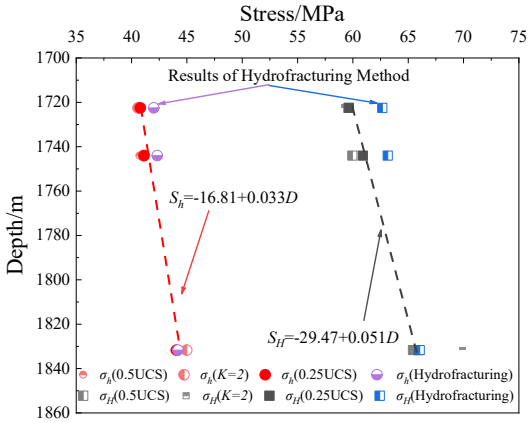

Figure 14. Comparison of horizontal principal stress versus depth obtained by the ASR method and the hydraulic fracturing technique.

As shown in Figure 14, the distribution patterns of the in-situ stress data measured by the

ARTICLE IN PRESS

two methods are similar, with good consistency in their variations with depth. The ASR method's in-situ stress curve lies to the left of the hydraulic fracturing method's curve, indicating generally lower values. The in-situ stress calculated using the ASR compliance ratio under 0.25 UCS stress conditions is closest to the hydraulic fracturing method results, with the maximum principal stress deviating by 0.14% to 4.1%, and the minimum principal stress deviating by 0.27% to 4.57%. When using a compliance ratio of $J_{aS}(t)/J_{aV}(t)=2$, the deviation in the maximum principal stress ranges from 5.3% to 5.8%, and the deviation in the minimum principal stress ranges from 2.3% to 4.25%. Therefore, in this ASR-based in-situ stress calculation, using a 0.25 UCS stress loading condition results in more accurate measurement outcomes.

Regression analysis of the in-situ stress data obtained using the ASR method yields depth-dependent equations for the maximum and minimum horizontal principal stresses as well as the vertical principal stress, as presented in Equation (6).

$$\begin{aligned}\sigma_H &= -29.47 + 0.051D \\ \sigma_h &= -16.81 + 0.033D \\ \sigma_v &= -51.93 + 0.056D\end{aligned} \quad (6)$$

Where, D denotes the burial depth of the measurement point (positive downward), expressed in meters.

ARTICLE IN PRESS

4.5 Mechanistic Insights into the Stress-Dependent ASR Compliance of Deep Granite

Natural rocks, as typical heterogeneous materials, contain numerous internal defects of varying degrees and characteristics. Their heterogeneity can be characterized using the deformation spatial variation coefficient[29]. For the deep granite from the Sanshandao Gold Mine ultra-deep shaft region (-1710m to -1831m), Brazilian splitting tests yielded deformation spatial variation coefficients ranging from 0.11 to 0.31, indicating that the granite in this region exhibits a notable degree of heterogeneity. Further examination using polarized light microscopy was conducted on thin sections of the granite, with representative micrographs shown in Figure 15. Under plane-polarized light, the granite appears gray with diverse mineral morphologies. The primary structural features include irregular porphyritic textures, massive

ARTICLE IN PRESS

structures, and granitic textures. The major mineral components are quartz, orthoclase, plagioclase, and biotite, with minor accessory minerals such as chlorite.

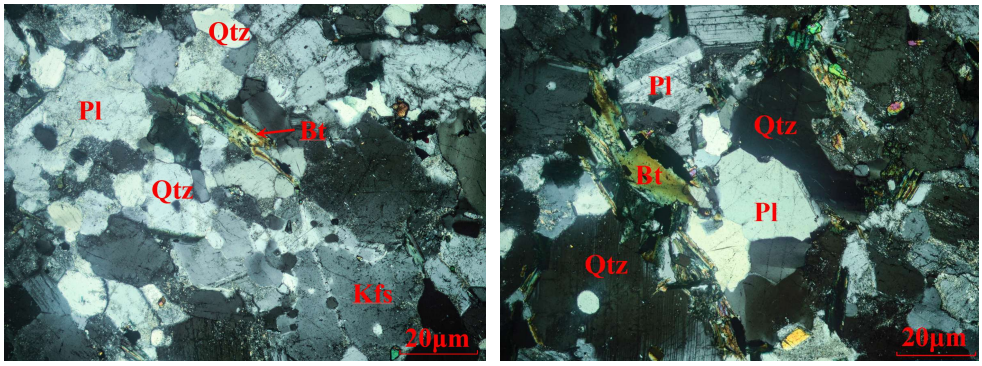

Figure 15. Microscopic Image of Granite.

The mineral volume content statistics of the granite samples indicate that the primary minerals are quartz (approximately 44.85% by volume) and plagioclase (45.56%). Secondary minerals include orthoclase (approximately 5.92%) and biotite (approximately 1.33%), while accessory minerals include calcite (approximately 0.69%) and trace amounts of minerals such as muscovite (approximately 1.65%). In deep, high-stress strata, weak minerals such as biotite and calcite, due to their lower strength, are more prone to plastic deformation and shear slip under external loading, exhibiting typical ductile deformation characteristics. In contrast, minerals like quartz and feldspar, which have relatively higher strength, are more likely to undergo brittle fracture under high-stress conditions, showing distinct brittle failure behavior. Thus, deep granite is composed of a variety of minerals with varying strengths. The spatial distribution and content differences of the mineral components result in significant variations in the rupture patterns and damage mechanisms under external forces.

Elevated in-situ stress magnitudes and increasingly intricate geological conditions are intrinsically linked to greater burial depths. The observed degradation in elastic modulus and acoustic velocity underscores the fact that persistent high geostress triggers significant micro-damage—either at inter-granular boundaries or within secondary mineral phases—due to the mechanical heterogeneity between mineral constituents. Furthermore, at depths surpassing 1,000 m, the inherent energy accumulation within the strata of the Sanshandao Gold Mine

ARTICLE IN PRESS

exhibits a quadratic growth pattern[30]. Notably, the energy density at -1831 m is roughly 1.42 times higher than that at -1722 m. Upon borehole stress relief, this stored energy acts as a driver for microscopic damage propagation, which eventually manifests as macroscopic anelastic strain. Therefore, rock samples retrieved from greater depths are more susceptible to irreversible structural reconfiguration and flaw coalescence during laboratory loading cycles (e.g., 0.5 UCS). This phenomenon explains the more prominent stress-dependent characteristics observed in the ASR compliance of deep-seated rock masses.

To delineate the correspondence between damage evolution and anelastic strain recovery, AE signals recorded during the ASR process were processed, with specimen ASR-2 serving as a representative case (Figure. 16). The temporal evolution of ASR is categorized into three distinct phases: rapid recovery (0–24 h), transitional attenuation (24–65 h), and the steady state (>65 h). In the initial rapid phase (0–24 h), the steep ascent of the ASR curve aligns with a surge in cumulative AE events and energy release, while RA values are predominantly confined to the 0–4 ms/dB interval. This synchronicity between low RA values and rising AE activity suggests that internal energy liberation triggers incompatible elastic rebound between heterogeneous mineral phases, thereby precipitating tensile micro-fractures. Hence, the incipient ASR stage is primarily characterized by brittle tensile damage. During the subsequent transition (24–65 h), the attenuation of residual stress leads to a diminishing recovery rate, with AE signatures shifting toward lower intensity ranges. This underscores the cessation of macro-scale tensile fracturing as the rock transitions from brittle failure toward a frictional-adjustment-based static equilibrium. In the final steady state (>65 h), both strain recovery and AE activity plateau, indicating that internal energy is fully dissipated and further damage is inhibited. Consequently, the ASR process is manifested as a progressive accumulation of damage through the continuous nucleation and expansion of internal cracks.

ARTICLE IN PRESS

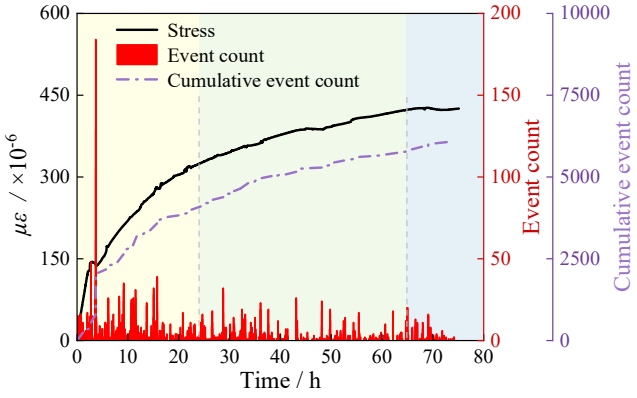

(a) Time-strain-AE event count variation curve

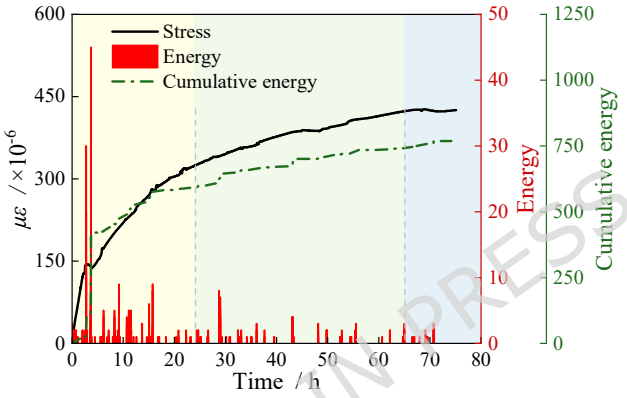

(b) Time-strain-AE energy variation curve

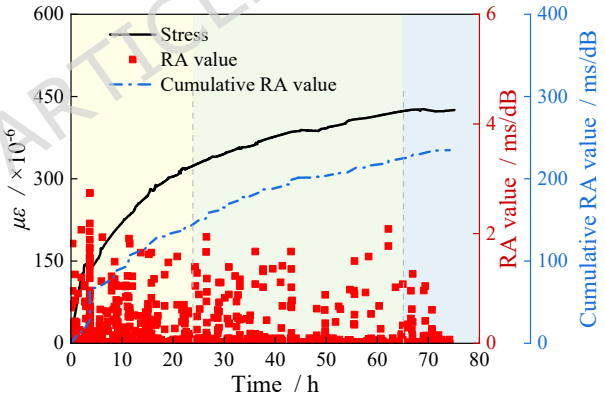

(c) Time-strain-RA value variation curve

Figure 16. AE characteristics of rock samples during ASR process.

In the process of ASR compliance calibration, elevated stress magnitudes facilitate substantial plastic deformation within secondary mineral phases, which consequently triggers stress-dependent fluctuations in ASR compliance across varying temporal and mechanical conditions. Accordingly, the implementation of the ASR technique in the Sanshandao ultra-

ARTICLE IN PRESS

deep shaft project necessitates a rigorous alignment between laboratory protocols and the in-situ geostress environment. Specifically, when determining the key parameters $J_{aS}(t)$ and $J_{aV}(t)$, the laboratory stress levels should be synchronized with the field-specific σ_v / UCS ratio. Additionally, maintaining a loading-unloading interval of at least 48 hours is essential to effectively mimic real-world stress regimes. Adhering to these criteria ensures the reliability of the calibration process, ultimately leading to higher precision in quantifying the in-situ stress field at great depths.

5 Discussion

The findings derived from this study, grounded in both laboratory and in-situ data from the Sanshandao Gold Mine, suggest that a calibration stress of 0.25 UCS significantly enhances the precision of ASR in-situ stress determination. This recommendation is particularly relevant for deep-seated, high-stress granitic massifs sharing similar geological attributes. The stress-dependent nature of granite ASR compliance is fundamentally rooted in its micromechanical evolution; specifically, the heterogeneous anelastic responses of mineral constituents and structural defects under varying loads manifest as macroscopic fluctuations in compliance. Thus, aligning laboratory calibration stress with the core's native stress regime is paramount for reliable ASR measurement.

Despite these insights, the applicability of the specific 0.25 UCS threshold may be constrained in geological settings with markedly different lithologies, mineralogies, or tectonic frameworks. To develop a more generalized framework for calibration stress selection, future investigations—especially for ultra-deep or highly anisotropic rock masses—must integrate uniaxial, conventional triaxial, and true triaxial testing. Such efforts will be critical in elucidating the complex stress-dependence of ASR compliance across a broader spectrum of geomechanical environments.

ARTICLE IN PRESS

6 Conclusions

To address the challenges of in-situ stress measurement in ultra-deep metal mine shafts, a series of ASR compliance experiments were conducted on deep core samples. The study revealed that under different uniaxial stress conditions, the shear and volumetric ASR compliance of deep granite, as well as their ratios, exhibit variations that reflect stress-dependent characteristics. Taking the Sanshandao Gold Mine ultra-deep shaft project as a case study, methodological improvements were proposed to enhance the accuracy of ASR-based stress measurements. The main conclusions are summarized as follows:

(1) Laboratory ASR compliance tests showed that, under the same uniaxial stress level, the shear and volumetric ASR compliance of three sets of rock samples tended to stabilize after 48 hours of unloading, despite variations in stress holding time. Prolonging the stress holding duration reduced the rate of anelastic strain recovery following unloading. Under different stress levels (0.25 UCS and 0.5 UCS), the ASR compliance and compliance ratios in both shear and volumetric modes changed across all sample sets, indicating a clear dependence on applied stress.

(2) Field ASR measurements were conducted in deep boreholes of the Sanshandao gold mine shaft. Results demonstrated significant anelastic strain recovery in the cores, reaching a stable peak at approximately 72 hours. In-situ stress values calculated using ASR compliance calibrated in the laboratory were compared with those from hydraulic fracturing tests. The two methods yielded similar stress distribution trends and showed strong consistency with depth. The stress values computed using ASR compliance ratios determined under a 0.25 UCS loading condition were the most consistent with hydraulic fracturing results, with differences of 0.14%–4.1% for maximum principal stress and 0.27%–4.57% for minimum principal stress.

(3) The inherent heterogeneity in mineralogy and fabric types of deep-seated granite, along with the distinct mechanical properties of its constituents, significantly dictates the response of ASR compliance to different stress regimes. Consequently, implementing the ASR technique at great depths necessitates a comprehensive evaluation of the stress-dependent characteristics of ASR compliance relative to the in-situ stress field. To optimize the precision and fidelity of

ARTICLE IN PRESS

geostress determination, the calibration of shear ($J_{aS}(t)$) and volumetric ($J_{aV}(t)$) compliance parameters should be synchronized with the field-specific σ_v / UCS ratio. Additionally, maintaining a minimum loading-unloading interval of 48 hours is crucial for capturing the time-dependent mechanical behavior required for a representative calibration.

Data availability

The datasets used and/or analysed during the current study available from the corresponding author on reasonable request.

References

1. Cai, M. F., QIAO, L., LI, H. B. *Principle and Technology of In-situ Stress Measurement* (Beijing: Science Press, 1995).

2. He, M. C., Xu, M. Research and development of hems cooling system and heat-harm control in deep mine. *Chinese Journal of Rock Mechanics and Engineering*. 2008; **27**(7): 1353.

3. He, M. C., Xie, H. P., Peng, S. P. Jiang, Y. D. Study on rock mechanics in deep mining engineering. *Chinese Journal of Rock Mechanics and Engineering*. 2005; **24**(16): 2803.

4. Guo, P. Y., Bu, M. H., Zhang, P. He, M. C. Research progress on the prevention and utilization of mine geothermal energy. *Chinese Journal of Engineering*. 2022; **44**(10): 1632-1651.

5. Xie, H. P., Gao, F., Ju, Y. Research and development of rock mechanics in deep ground engineering. *Chinese Journal of Rock Mechanics and Engineering*. 2015; **34**(11): 2161-2178. doi:10.13722/j.cnki.jrme.2015.1369

6. Kang, H. P., Lin, J., Zhang, X. Research and application of in - situ stress measurement in deep mines. *Chinese Journal of Rock Mechanics and Engineering*. 2007; **05**: 929-933.

7. Voight, B. Determination of the virgin state of stress in the vicinity of a borehole from measurements of a partial anelastic strain tensor in drill cores. *Felsmechanik and Ingenieurgeologie*. 1968; **6**: 201-215.

ARTICLE IN PRESS

8. Teufel, L. W., Warpinski, N. R. An Assessment of the Factors Affecting Hydraulic Fracture Containment in Layered Rock: Observations from a Mine back Experiment. *Hydraulic facturing and geothermal energy*. Springer Netherlands; 1983.

9. Matsuki, K. Three-dimensional in situ stress measurement with anelastic strain recovery of a rock core. Proc 7th ISRM International Congress on Rock Mechanics. International Journal of Rock Mechanics and Mining Sciences & Geomechanics Abstracts. 1992; **29**(5).

10. Matsuki, K., Takeuchi, K. Three-dimensional in situ stress determination by anelastic strain recovery of a rock core. *International Journal of Rock Mechanics and Mining Sciences & Geomechanics Abstracts*. 1993; **30**(7).

11. Lin, W. R., Yeh, E. C., Ito, H. Preliminary Results of Stress Measurement Using Drill Cores of TCDP Hole-A: An Application of Anelastic Strain Recovery Method to Three - Dimensional In-Situ Stress Determination. *Terrestrial, Atmospheric and Oceanic Sciences*. 2007; **18**(2).

12. Lin, W. R. A Core - Based Method to Determine Three-Dimensional In - Situ Stress in Deep Drilling Wells: Anelastic Strain Recovery Technique. *Chinese Journal of Rock Mechanics and Engineering*. 2008; **27**(12): 2387-2394.

13. Sun, D. S. et al. Three-Dimensional in Situ Stress Determination by Anelastic Strain Recovery and Its Application at the Wenchuan Earthquake Fault Scientific Drilling Hole1(WFSD-1). *Science China: Earth Sciences.* 2014; **44**(3): 510-518.

14. Sun, D. S. et al. In Situ Stress Measurement by ASR Method of Scientific Drilling No 1 Hole in Wenchuan Earthquake Fault Zone. *Geology in China*. 2013; **40**(3): 840-845.

15. Cui, J. W. et al. Determination of Three-Dimensional in Situ Stresses from Anelastic Strain Recovery(ASR)of Wenchuan Earthquake Fault Scientific Drilling Project Hole-1(WFSD-1)and Formation Mechanism of the "5.12 Wenchuan Earthquake. *Acta Petrologica Sinica.* 2013; **29**(6): 2033-2047.

16. Wang, L. J. et al. Determination of Three-Dimensional In-Situ Stresses by Anelastic Strain Recovery in Tengchong Scientific Drilling Hole. *Acta Geoscientica Sinica*. 2016; **37**(1): 111-115.

17. Wang, L. J. et al. Anelastic Strain Recovery Method to Determine In Situ Stress and Application Example. *Chinese Journal of Geophysics.* 2012; **55**(5): 1674-1681.

ARTICLE IN PRESS

18. Li, Z. J. Measurement of in - situ stress by ASR method and analysis of stress field inversion in a tunnel of Sichuan - Tibet railway. [Doctoral dissertation]. Yanshan University; June 2021.

19. Chen, T. X. Research on in - situ stress measurement and application based on inelastic strain recovery. [Doctoral dissertation]. Yanshan University; June 2020.

20. Zhang, X. L., Ying, L., Zhao, D. A. Application of In-Situ Stress Measurement Technology of Ultra Deep Survey Borehole ASR Method. *Journal of Jilin University (Earth Science Edition)*. 2024; **54**(1): 198-207. doi:10.13278/i.cnkijiuese.20220118

21. Matsuki, K. Anelastic strain recovery compliance of rocks and its application to in situ stress measurement. *International Journal of Rock Mechanics & Mining Sciences*. 2008; **45**: 952–965.

22. Sun, D. S. Experimental study of anelastic strain recovery in - situ stress measurement methods and its application. [Doctoral dissertation]. Chinese Academy of Geological Sciences; May 2014.

23. Gong, B., Tang, C. A., Wang, S. Y., Bai, H.M., Li Y. C. Simulation of the nonlinear mechanical behaviors of jointed rock masses based on the improved discontinuous deformation and displacement method. *International Journal of Rock Mechanics and Mining Sciences.* 2019; **122**: 104076.

24. Su, X. B. Fracture evolution mechanism and energy release mechanism of heterogenerous rock materials under high stress state. [Doctoral dissertation]. Beijing: University of Science and Technology Beijing; 2022.

25. Yin, X. C. *Solid Mechanics* (Seismological Press; 2011).

26. Liu, Y. Ultrasonic time domain and frequency domain characteristics of deep granite damage evolution and ASR measurement. [Doctoral dissertation]. University of Science and Technology Beijing; June 2022. doi:10.26945/d.cnki.gbjku. 2022. 000200.

27. Matsuki, K. Anelastic strain recovery compliance of rocks and its application to in situ stress measurement. *International Journal of Rock Mechanics and Mining Sciences*. 2008; **45**(6): 952–965.

28. Suggested methods for rock stress determination. *International Journal of Rock Mechanics and Mining Sciences & Geomechanics Abstracts*. 1987; **24**(1).

29. Ji, H. G., Fu, Z., Zhang, Y. Z. Zhang C. Y., Chen. D. S. Critical energy distribution and fracture

ARTICLE IN PRESS

ARTICLE IN PRESS

characteristics of heterogeneous rock under splitting condition. *Journal of China Coal Society*. 2024; **49**(S2): 756−771. doi:10.13225/j.cnki.jccs.2024.0432.

30. Fu, Z. Research on the synergistic bearing mechanism and performance evaluation of rock-concrete composite grouting stop structure in deep shaft working face of metal mines. [Doctoral dissertation]. University of Science and Technology Beijing; July 2025. DOI:10.26945/d.cnki.gbjku. 2025. 000310.

Acknowledgements

This research is supported by The National Key Research and Development Program of China [Grant No.2023YFC2907400. No. 2023YFC2907403].

Funding

This work was funded by National Key Research and Development Program of China, 2023YFC2907400, 2023YFC2907403.

ARTICLE IN PRESS